

Principle Investigation of Structural, Electronics and Chemical Properties of Sn Doped PbX (X=S, Se, Te)

Asghar Khan M¹, Zulfiqar Ali Shah^{2*}, Jabran Khan¹, Yasir Arafat³, Sikandar Hayat¹ and Munawar Saeed⁴

¹Department of Physics, Hazara University, Mansehra, Pakistan

²Department of Physics, Khwaja Fareed University of Engineering and IT, Rahim Yar Khan, 64200, Pakistan

³Department of Computer Science Government College University Faisalabad, Layyah Campus, 31300 Pakistan

⁴Department of Chemistry, Khwaja Fareed University of Engineering & Information Technology, Rahim Yar Khan, 64200 Pakistan

Abstract

The Structural, electronic and chemical bonding of the Sn doped PbX (X=S, Se, Te) are calculated by full potential linearized augmented plane wave method (FP-LAPW) within density functional theory (DFT). Generalized gradient approximation of Wu and Cohen (WC-GGA) is used for calculating the exchange correlation effects. The structural parameters changes with respect to doping. The calculations show that the band gap decreases with the increase of Sn concentration. It has observed that the s, p and d states of PbX (X=S, Se, Te) control their electronic properties. The alloys $Pb_{1-x}Sn_xS$, $Pb_{1-x}Sn_xSe$ and $Pb_{1-x}Sn_xTe$ show covalent bonding nature which enhances by increasing the Sn concentration.

Keywords: Density functional theory; Generalized gradient approximation; Density of state; Structural properties; Electronic properties

Introduction

Computational materials science is an emerging field in condensed matter physics. Computational techniques have come to the level of experiment nowadays. One can determine the physical properties of a material even without the information of experimental data [1,2]. The recent development of computational power allows one to study very complex systems.

In 1874, IV-VI semiconductors were started to be utilized in solid state electronic devices after the Ferdinand Braun's report on electrical rectification by PbS [3]. After this discovery, PbS also utilized as a rectifier in radios. In recent era, the IV-VI semiconductors have many applications in optoelectronic devices which are mainly utilized for emission and detection of mid-infrared radiations. The IV-VI semiconductors consist of binary compounds PbS, PbSe, and PbTe and their alloys i.e., PbSnSe, PbSnTe, PbSrSe, PbEuTe etc. [4]. They are used in diode lasers [5], long wavelength imaging [6], and in also thermo photovoltaic devices [7]. They are also utilized to control pollution and gas spectroscopy, remote sensing, thermograph, chemical sensing etc. [8,9].

At normal temperature and pressure Lead sulfide (PbS) rock-salt structure is a narrow band gap semiconductor material. Its band gap is direct and equal to 0.45 eV at room temperature [10]. Lead selenide (PbSe) is also a direct band gap semi-conductor material which has a stable rock-salt structure. The band gap of PbSe is equal to 0.16 eV at 4 K [11]. Lead telluride (PbTe) is direct band gap material and its band gap is equal to 0.29 eV. It also exists in rock salt structure at normal temperature and pressure [12]. Tin sulfide (SnS) is a narrow indirect band gap of 1.07 eV and the direct band gap occurs at energy of 1.3 eV [13]. The structure of SnS is orthorhombic but it changes to rock-salt structure at high temperature. Tin selenide (SnSe) is also an orthorhombic crystal and become rock-salt at high temperature as well [14]. Tin chalcogenide (SnTe) is a narrow direct band gap semiconductor with a value of 0.35 eV. It exists in rock-salt (RS) structure at ambient conditions [15].

With doping Sn in PbX (X=S, Se, Te), ternary compounds $Pb_{1-x}Sn_xTe$, $Pb_{1-x}Sn_xSe$, $PbS_{1-x}Se_x$ have been experimentally grown at various

concentrations [9]. These materials are widely used for optoelectronic applications e.g., photovoltaic sensors. These photovoltaic IV-VI semiconductor infrared sensors ($Pb_{1-x}Sn_xTe$, $Pb_{1-x}Sn_xSe$, $PbS_{1-x}Se_x$, PbTe etc.) are as sensitive as $Hg_{1-x}Cd_xTe$, and can fabricate easily especially on Si substrates. However, the technology of photovoltaic lead compound selection is behind that of $Hg_{1-x}Cd_xTe$ alloy [9].

Computational techniques have many advantages in material science due to no restrictions in these techniques. We can easily model all types of materials by computational techniques. The ab-initio or first principle study is the approach to finding the various properties of a material by just knowing its structure and composition [16]. This technique has an advantage over real experiment because we have all controls over all variables in material for stimulations. This control helps us to design a practicable experiment for understanding the material's behavior on a specific variable. From this calculation, it is very easy to change the crystal structure, remove or substitute an atom, varying pressure and other changes which will alter on the properties of the material.

Density functional theory (DFT) [17] is usually used to investigate the electronic and structure properties of materials, it can also predict chemical, optical and magnetic properties of the materials i.e., metals, semi-metals, semiconductors and insulators. The density functional theory (DFT) was proposed by Hohenberg and Kohn to simplify the problem and got the noble price in chemistry in 1998. The density functional theory (DFT) is one of the important tools in computational material science for investigation of properties of material such as optical, structural, electronic and magnetic.

***Corresponding author:** Zulfiqar Ali Shah, Department of Basic Sciences and Humanities, Khwaja Fareed University of Engineering and IT, Rahim Yar Khan, Pakistan, Tel: +92689239122; E-mail: szulfiqar01@yahoo.com

Received August 31, 2017; **Accepted** September 12, 2017; **Published** September 16, 2017

Citation: Asghar Khan M, Shah ZA, Khan J, Arafat Y, Hayat S, et al. (2017) Principle Investigation of Structural, Electronics and Chemical Properties of Sn Doped PbX (X=S, Se, Te). J Theor Comput Sci 4: 159. doi:10.4172/2376-130X.1000159

Copyright: © 2017 Asghar Khan M, et al. This is an open-access article distributed under the terms of the Creative Commons Attribution License, which permits unrestricted use, distribution, and reproduction in any medium, provided the original author and source are credited.

Computational Details

This project is completed by performing the calculations through WIEN2K code. This software is based on DFT. FP-LAPW model is utilized in the Wien2k code [18], with different XC- potential. The main two parts are consisting in the Wien2k code. The first is the initialization and the second is the self consistent-field cycle (SCF). Then in every part there are still many programs which will be done step by step to complete these cycles and can be able to find the structural, electronic and Chemical properties of $Pb_{1-x}Sn_xS$, $Pb_{1-x}Sn_xSe$ and $Pb_{1-x}Sn_xTe$ compounds at concentrations $x=0, 0.25, 0.5, 0.75, 1$.

Results and Discussion

Structural properties

The calculated structural properties of the studied materials are lattice constant a (\AA), Bulk modulus B (Gpa), derivative of bulk modulus B' , unit cell energy E_0 . Before the discussion of structural properties of ternary compounds $Pb_{1-x}Sn_xS$, $Pb_{1-x}Sn_xSe$ and $Pb_{1-x}Sn_xTe$ at concentrations $x=0, 0.25, 0.5, 0.75, 1$, we first start the structural properties of binary compounds PbS , $PbSe$, $PbTe$, SnS , $SnSe$ and $SnTe$ in rock-salt phase. The Birch-Murnaghan's equation [19] is used to minimize the total energy with respect to unit cell volume which is given as:

$$E(V) = E_0 + \frac{9V_0B_0}{16} \left\{ \left[\left(\frac{V_0}{V} \right)^{\frac{2}{3}} - 1 \right] B_0 + \left[\left(\frac{V_0}{V} \right)^{\frac{2}{3}} - 1 \right]^2 \left[6 - 4 \left(\frac{V_0}{V} \right)^{\frac{2}{3}} \right] \right\} \quad (1)$$

The structure of all binary compounds PbS , $PbSe$, $PbTe$, SnS , $SnSe$, $SnTe$ and ternary compounds $Pb_{1-x}Sn_xS$, $Pb_{1-x}Sn_xSe$ and $Pb_{1-x}Sn_xTe$ are in sodium chloride (rock-salt) structure. The sodium chloride structure represented a face centered cubic lattice. The structure of binary compounds and ternary compounds are shown in Figure 1. Plots of total energy as a function of volume of $Pb_{1-x}Sn_xS$, $Pb_{1-x}Sn_xSe$ and $Pb_{1-x}Sn_xTe$ at different concentration of Sn gives unit cell volume V , lattice constant a (\AA), Bulk modulus B (Gpa), derivative of bulk modulus B' and unit cell energy E_0 as shown in Figure 2. So the lattice constant and bulk modulus values are in good agreement with experimental values as shown in Tables 1 and 2 and from the tables lattice constant is decreasing as we adding the concentration of Tin (Sn) in PbX ($X=S, Se, Te$). The maximum lattice constant is at zero doping in the PbX ($X=S, Se, Te$) and minimum at the doping concentration of $x=1$. In $Pb_{1-x}Sn_xS$ the bulk modulus is maximum when Sn is doped at the concentration of $x=1$ and minimum when the Tin (Sn) is doped at concentration of $x=0$.

Also the energy of $Pb_{1-x}Sn_xS$ is maximum at concentration of $x=0.25$ and minimum at the doping concentration of Tin (Sn) at $x=1$ as shown in Table 1. In $Pb_{1-x}Sn_xSe$ the bulk modulus is maximum at doping concentration of $x=1$ and minimum at the doping concentration of $x=0.25$. Also the energy of $Pb_{1-x}Sn_xSe$ is maximum at concentration of $x=0.25$ and minimum at concentration of $x=1$ as shown in Table 2. In $Pb_{1-x}Sn_xTe$ the bulk modulus is maximum at concentration of $x=1$ and minimum at doping concentration of Tin (Sn) at $x=0.25$ as shown in Table 3. The energy of $Pb_{1-x}Sn_xTe$ is maximum at concentration of $x=0.25$ and minimum at concentration of $x=1$. The bulk modulus and energy of $Pb_{1-x}Sn_xSe$ and $Pb_{1-x}Sn_xTe$ are changing in same way as in both samples the bulk modulus is maximum at concentration of $x=1$ and minimum at concentration of $x=0.25$, also in the energy case in both samples it is maximum at concentration of $x=0.25$ and minimum at concentration of $x=1$ but the parameters i.e., bulk modulus and energy of $Pb_{1-x}Sn_xS$ is changing in different concentration then $Pb_{1-x}Sn_xSe$ and

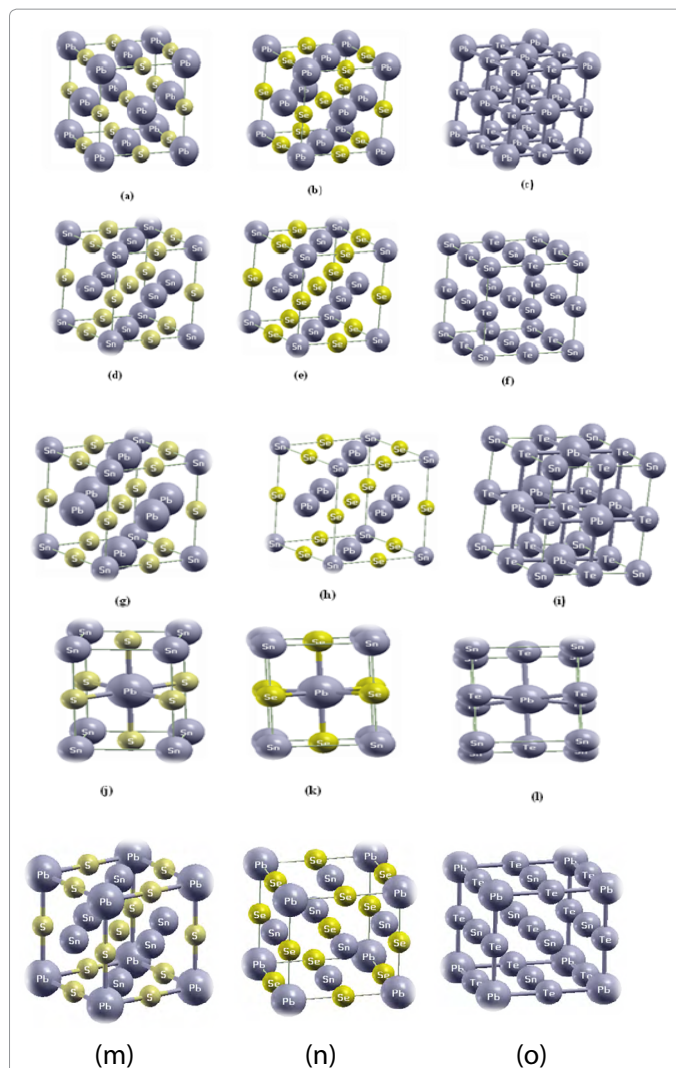
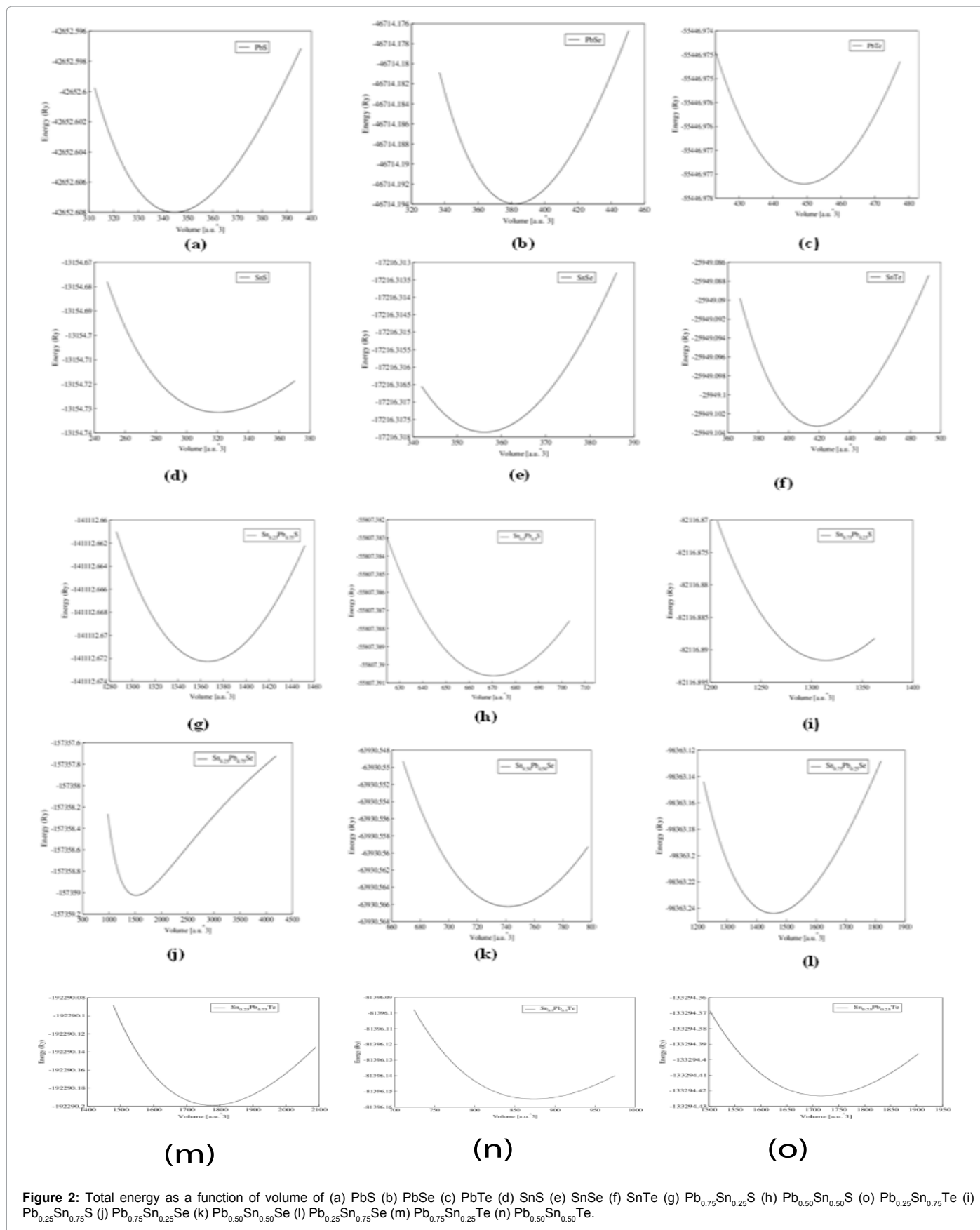


Figure 1: Structure of (a) PbS (b) $PbSe$ (c) $PbTe$ (d) SnS (e) $SnSe$ (f) $SnTe$ (g) $Pb_{0.75}Sn_{0.25}S$ (h) $Pb_{0.75}Sn_{0.25}Se$ (i) $Pb_{0.75}Sn_{0.25}Te$ (j) $Pb_{0.5}Sn_{0.5}Se$ (k) $Pb_{0.5}Sn_{0.5}S$ (l) $Pb_{0.5}Sn_{0.5}Te$ (m) $Pb_{0.25}Sn_{0.75}S$ (n) $Pb_{0.25}Sn_{0.75}Se$ (o) $Pb_{0.25}Sn_{0.75}Te$.

$Pb_{1-x}Sn_xTe$. In the Figure 3, it shows that lattice constant varies with respect to doping concentration of Tin (Sn).

Electronic properties

Band structure: The band structure gives useful information about the structure of materials. The band structure of Sn doped PbX ($X=S, Se, Te$) compounds at different concentration are calculated and shown in Figures 4a-4o respectively. For PbS the band structure is shown in Figure 4a which is in rock salt phase, from figure the minimum of conduction band (CB) and the maximum of valance band (VB) are at L-symmetry point so PbS has a direct band of 0.28 eV. Similarly of $PbSe$ and $PbTe$ have same L-symmetry point and have direct band gaps of 0.48 eV and 0.8 eV as shown in Figures 4b and 4c. From Figures 4d-4f it is clear that SnS , $SnSe$ and $SnTe$ have narrow direct band gap values 0.09 eV, 0.1 eV and 0.07 eV respectively. The compounds $Pb_{0.75}Sn_{0.25}S$, $Pb_{0.75}Sn_{0.25}Se$ are zero band gap material as shown in Figure 4g and 4j. The $Pb_{0.75}Sn_{0.25}Te$ has a narrow direct band gap 0.082 eV as shown in Figure 4m. In $Pb_{0.50}Sn_{0.50}S$, $Pb_{0.25}Sn_{0.75}S$, $Pb_{0.50}Sn_{0.50}Se$, $Pb_{0.25}Sn_{0.75}Se$, $Pb_{0.50}Sn_{0.50}Te$ and $Pb_{0.25}Sn_{0.75}Te$ compounds have zero bands gap



	a(A°)	B(GPa)	B'	E ₀ (Ry.)
PbS				
This work	5.8893	60.7348	7.13	-42652.61
Other works	6.012 ^d	52.1 ^d	4.10 ^e	-
Experiment	5.95 ^a	52.9 ^d	-	-
Pb_{0.75}Sn_{0.25}S	5.8717	62.26	5.0	-141112.67
This work				
Other works				
Experiment				
Pb_{0.50}Sn_{0.50}S	5.835	60.08	5.0	-111614.78
This work				
Other works				
Experiment				
Pb_{0.25}Sn_{0.75}S	5.796	62.01	4.12	-82116.89
This work				
Other works				
Experiment				
SnS	5.7492	64361	4.034	-13154.73
This work				
Other works	5.848 ^c			
Experiment	5.69 ^b			

^aRef [20], ^bRef [21], ^cRef [22], ^dRef [23], ^eRef [24].

Table 1: Calculated structural parameters of Sn doped PbX(X=S) at variation of Sn concentration along with experimental and other calculations.

	a(A°)	B(GPa)	B'	E ₀ (Ry.)
PbSe				
This work	6.095	56.6262	4.5911	-46714.19
Other works	6.222 ^a	47.5 ^a , 49.1 ^a	4.35 ^c	-
Experiment	6.117 ^a	54.1 ^a	-	-
Pb_{0.75}Sn_{0.25}Se	6.081	52.5234	4.4792	-157359.025
This work				
Other works				
Experiment				
Pb_{0.50}Sn_{0.50}Se	6.035	55.94	4.12	-127861.13
This work				
Other works				
Experiment				
Pb_{0.25}Sn_{0.75}Se	5.997	56.2424	4.4051	-98362438
This work				
Other works				
Experiment				
SnSe	5.954	60798	5.0	-17216.3178
This work				
Others works	6.062 ^b			
Experiment	5.90 ^d			

^aRef [23], ^bRef [22], ^cRef [24], ^dRef [25].

Table 2: Calculated structural parameters of Sn doped PbX(X=Se) at variation of Sn concentration along with experimental and other calculations.

as shown in Figure 4g, 4h, 4k, 4l, 4n and 4o. So the semiconductor materials become metallic at doping concentration of x= 0.25, 0.50, 0.75 but at doping concentration of x=1 then again there is again narrow band gap. All the band gap values for different compounds at different doping concentration are mentioned in the Table 4. As the band gap occurs in the range of 0-0.8 eV, the fundamental edge occurs in the infrared region. The result matches with experimental one because it's also show metallic nature at different doping concentrations as mentioned in Table 4 As there are less materials on the band gap of Sn doped PbX(X=S, Se, Te) with which we compare it with our results but we are confident about our results due to use of Wu-Cohen GGA at high k-point value of 5000.

Density of states: Density of states (DOS) describes the number of states of a system per unit interval of energy which are occupied by the electrons. Study of band structure, dielectric function, bond character

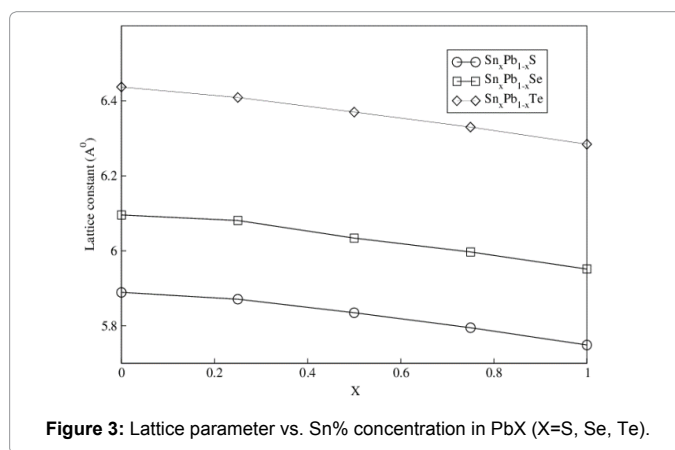


Figure 3: Lattice parameter vs. Sn% concentration in PbX (X=S, Se, Te).

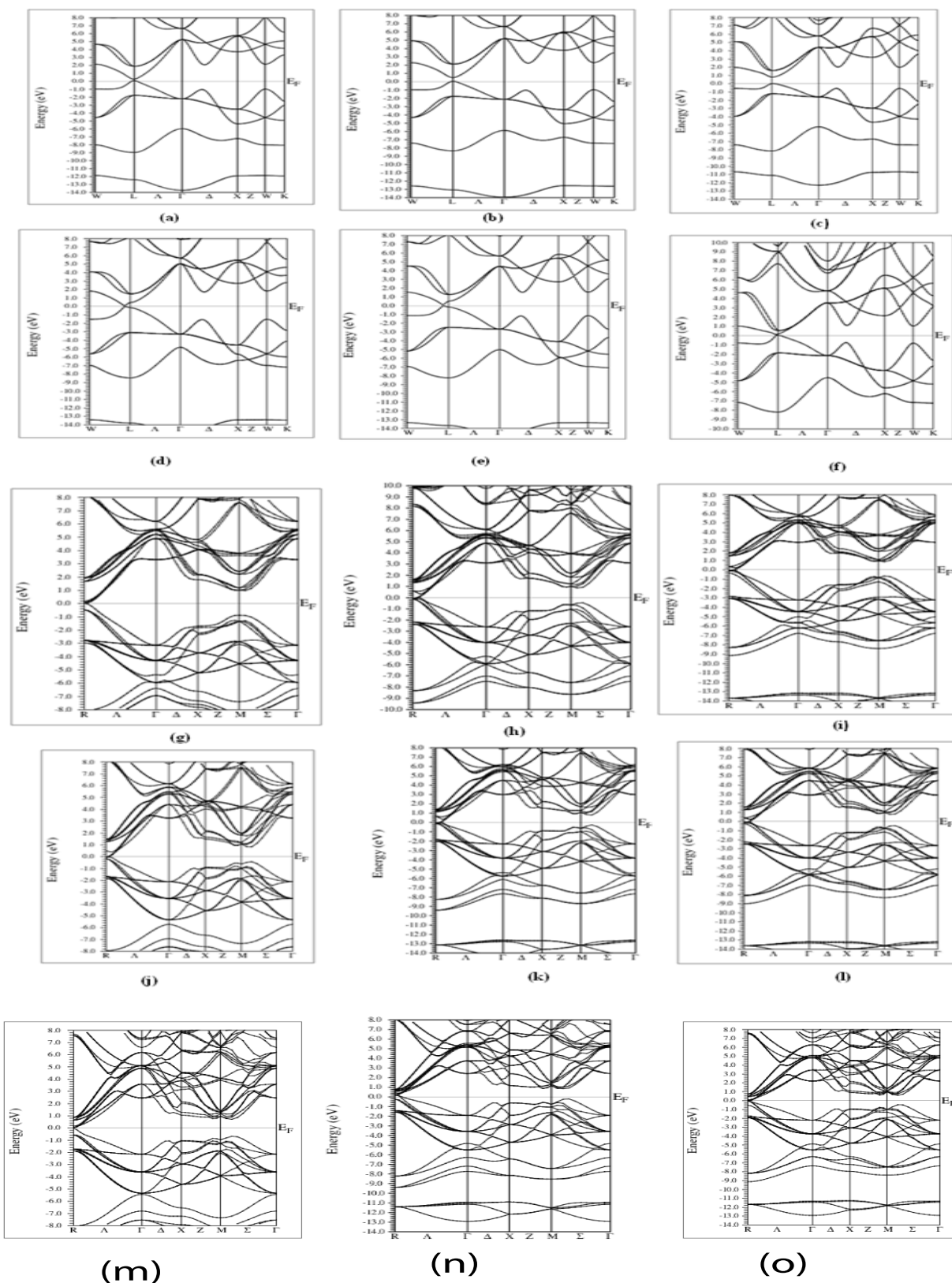


Figure 4: Band structure of (a) PbS (b) PbSe (c) PbTe (d) SnS (e) SnSe (f) SnTe (g) $\text{Sn}_{0.25}\text{Pb}_{0.75}\text{S}$ (h) $\text{Sn}_{0.50}\text{Pb}_{0.50}\text{S}$ (i) $\text{Sn}_{0.75}\text{Pb}_{0.25}\text{S}$ (j) $\text{Sn}_{0.25}\text{Pb}_{0.75}\text{Se}$ (k) $\text{Sn}_{0.50}\text{Pb}_{0.50}\text{Se}$ (l) $\text{Sn}_{0.75}\text{Pb}_{0.25}\text{Se}$ (m) $\text{Sn}_{0.25}\text{Pb}_{0.75}\text{Te}$ (n) $\text{Sn}_{0.50}\text{Pb}_{0.50}\text{Te}$ (o) $\text{Sn}_{0.75}\text{Pb}_{0.25}\text{Te}$.

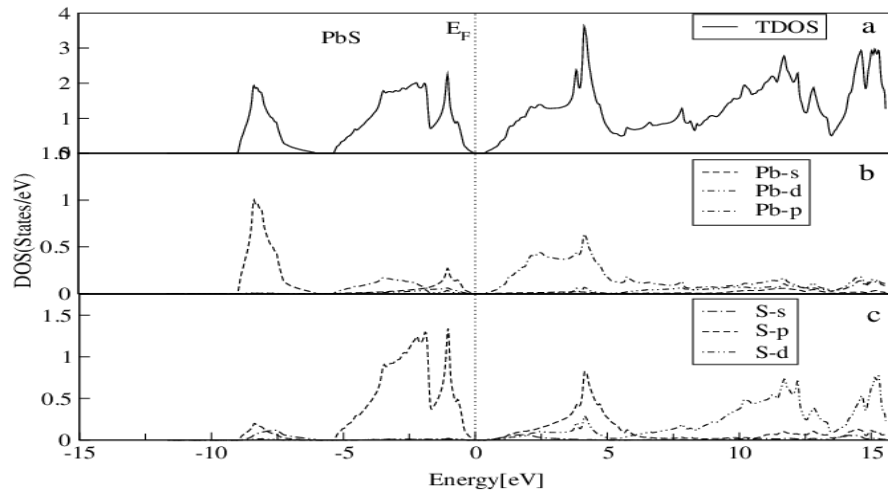


Figure 5: DOS of PbS.

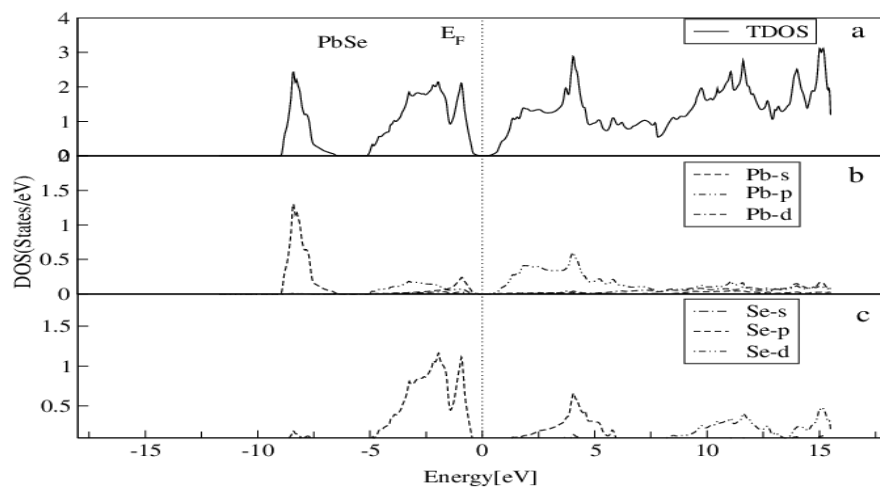


Figure 6: DOS of PbSe.

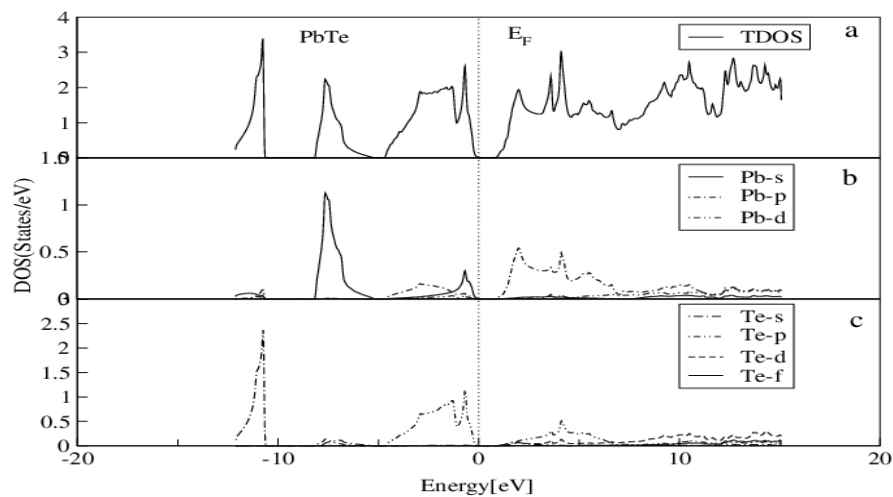


Figure 7: DOS of PbTe.

and reflectivity require the knowledge of electron density of states. The DOS of PbS, PbSe, PbTe, SnS, SnSe, SnTe and ternary compounds of $\text{Sn}_{0.50}\text{Pb}_{0.50}\text{S}$, $\text{Sn}_{0.50}\text{Pb}_{0.50}\text{Se}$ and $\text{Sn}_{0.50}\text{Pb}_{0.50}\text{Te}$ by using GGA scheme are shown in Figures 1 and 5-12. There are four regions in the fundamental density of states. The lower region of VB, the upper region of VB, the lower region of CB and the upper region of CB. DOS of PbS in rock salt are shown in Figure 5. The lower part of VB is started around -8.75 eV and the major contribution at this part is Pb-s state, also a little contribution by the states of S-s and s-p. Now the upper part of VB start about -5.8 eV. The VB near Fermi level is dominated by S-p and also a little contribution by the states of Pb-s and Pb-p. Now the third region is the CB in which the lower part dominated by Pb-p and S-p states and the upper part is due to S-d state.

For PbSe the lower part of VB is dominated by Pb-s state and also a little contribution of Se-p state. Then after the lower part is the upper part of VB which is near to the Fermi level and has a major contribution due to Se-p state and also a little contribution due to Pb-s, Pb-p, and Pb-d states. Then near to the Fermi level is the CB whose lower part is dominated by the Pb-p and Se-p states. For the upper part of CB the major contribution is due to Se-d state and also little contribution of Pb-s, Pb-p and Pb-d as shown in Figure 6.

DOS for PbTe is the lower part of CB, dominated by Te-s state and also little contribution due to Pb-s state is shown in Figure 7. The upper part of VB is dominated due to Te-p state and also little contribution of Pb-s, Pb-p, Pb-d states. Then in CB the lower part is dominated due to Pb-p and Te-p states and the small contribution is due to Pb-s, Pb-d and Te-d states. The upper level of CB is mainly contributed due to Pb-p and Te-d states.

From figure of SnS it is clear that the lower part of VB is dominated due to Sn-s state and small contribution of Sn-p, S-s and S-p states. Then the upper part is dominated due to Sn-s and S-s states and also small contribution is Sn-p state. The lower part of CB is dominated due to Sn-p and S-p states near the Fermi level and the upper part is dominated due to Sn-p, Sn-d and S-d states and also small contribution of Sn-S, Sn-f and S-p states as shown in Figure 8.

DOS of SnSe is shown in Figure 9. The lower part of VB is dominated by Sn-S state and also small contribution of Se-s, Se-p states. Then the

upper part has a major contribution of Sn-s and Se-p states and also small contribution of Sn-p and Sn-d states. Then the lower part of CB near the Fermi level is dominated by Sn-p and Se-p states and the upper part is dominated due to Sn-p and Se-d states and also small contribution of Sn-s, Sn-d, Sn-f, Se-s and Se-p states.

It is clear from Figure 10 that the lower part of VB is dominated by Te-s state and also small contribution of Sn-s and Sn-p states. The upper part of VB is due to Sn-s and Te-p states. After Fermi level is the lower part of CB which is dominated by Sn-p and Te-p states and for the upper part it is dominated by Sn-d and Te-d states.

For the compound $\text{Sn}_{0.50}\text{Pb}_{0.50}\text{S}$ the DOS is shown in Figure 11. The lower part of the VB is dominated due to Sn-s and Pb-s states and also small contribution of S-s and S-p states. Then the upper part of VB is dominated due to S-p state and also a small contribution of Sn-s, Pb-s, Sn-p, Pb-p and Pb-d states. Then for lower part of CB which is near to Fermi level is dominated by Sn-p, Pb-p and S-p states and also small contribution of Sn-s, Sn-d, Pb-d and S-d states. For upper part of CB is dominated by S-d state.

The DOS of $\text{Sn}_{0.50}\text{Pb}_{0.50}\text{Se}$ is shown in Figure 12. In figure the lower part of VB is dominated by Sn-s and Pb-s states and also small contribution of Se-s and Se-p states. Then after the lower part there is upper part of VB which has a major contribution of Se-p state and also small contribution of Sn-s, Sn-p, Pb-s and Pb-p states. The lower part of CB is dominated by Sn-p state and the upper part is dominated by Se-d state.

The lower Te-s state band is dominated and the small contribution of Sn-s and Pb-s states is shown in Figure 13. Then near Fermi level is the upper part of VB which is dominated by Pb-s and Te-p states and also small contribution of Sn-s, Sn-p and Pb-p states. After the Fermi level is the lower part of CB which is dominated by Sn-p and Pb-p states and also little contribution of Sn-s, Sn-d and Te-d states. The upper part of CB is dominated by Sn-d, Pb-d and Te-d states.

Electron density: The chemical bonding properties can be defined by the charge density distribution in a solid. The nature of bonding can be described by electron density i.e., ionic or covalent bond between the cation and anion. The electron density plots of Sn doped PbX(X=S,

	a(A°)	B(GPa)	B'	E ₀ (Ry.)
PbTe				
This work	6.43	44.44	5.0	-55446.977
Other works	6.55 ^c	39.95 ^c	4.32 ^c	-
Experiment	6.47 ^a	39.8 ^c	-	-
Pb_{0.75}Sn_{0.25}Te	6.409	46.1301	4.4436	-192290.1989
This work				
Other works				
Experiment				
Pb_{0.50}Sn_{0.50}Te	6.373	46.29	5.00	-162792.31
This work				
Other works				
Experiment				
Pb_{0.25}Sn_{0.75}Te	6.33	47.1526	4.6470	-133294.4232
This work				
Other works				
Experiment				
SnTe	6.28	50.0925	4.9679	-25949.032
This work	6.312 ^b			
Others works	6.327 ^d			
Experiment				

^aRef [26], ^bRef [22], ^cRef [24], ^dRef [27].

Table 3: Calculated structural parameters of Sn doped PbX(X=Te) at variation of Sn concentration along with experimental and other calculations.

		This work (GGA)	Experimental	Other Calculations
PbS				
Eg		0.28	0.42 ^c , 0.286 ^d	0.448 ^d , 0.380 ^d
Pb_{0.50}Sn_{0.50}S				
Eg		0		-
SnS				
Eg		0.09	-	-
PbSe				
Eg		0.48	0.278 ^b	0.318 ^d , 0.340 ^d
Pb_{0.50}Sn_{0.50}Se				
Eg		0	x=0...~0.2, 0.18-0 eV (T=77k) ^g	
SnSe				
Eg		0.1		
PbTe				
Eg		0.8	0.33 ^e , 0.19 ^e	0.649 ^e
Pb_{0.75}Sn_{0.25}Te				
Eg		0.082	x=0...~0.4, 0.22-0eV (T=77k) ^g	
Pb_{0.50}Sn_{0.50}Te				
Eg		0	x=0...~0.4, 0.22-0eV (T=77k) ^g	
SnTe				
Eg		0.07	0.35 ^a	0.19 ^f (300k)

Pb_{0.75}Sn_{0.25}S, Pb_{0.75}Sn_{0.25}Se, Pb_{0.25}Sn_{0.75}S, Pb_{0.25}Sn_{0.75}Se, Pb_{0.25}Sn_{0.75}Te are zero band gap due to our result. ^aRef [28], ^bRef [29], ^cRef [30], ^dRef [23], ^eRef [31], ^fRef [32], ^gRef [33]

Table 4: Energy band gaps (in eV) for Sn doped PbX (X=S, Se, Te) compounds at (0 ≤ X ≤ 1) in the rock salt phase along with the experimental and other calculations.

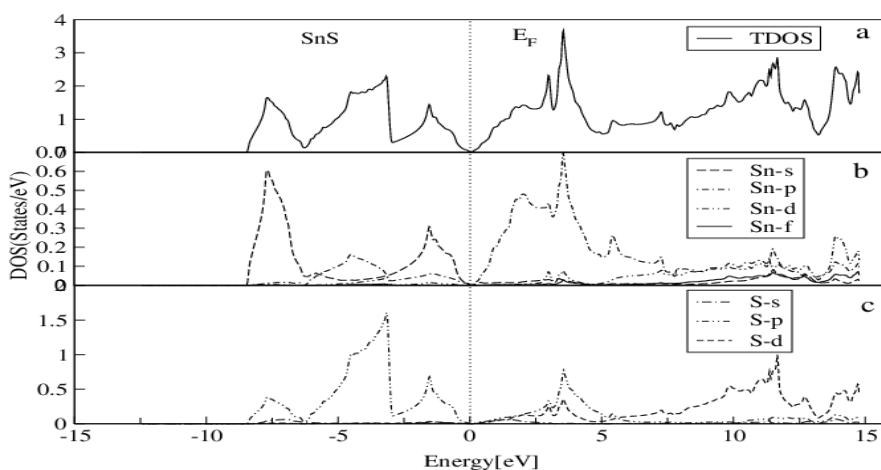


Figure 8: DOS of SnS.

Se, Te) at different concentration are shown in Figure 14a-14i. The electron density plots of these compounds are in rock salt phase at (110) plane. It is clear from figures that the electron density plot of compounds is covalent nature. By adding Sn concentration in the compounds PbX(X=S, Se, Te) the nature of covalent bond becomes stronger.

Conclusion

The Structural, electronic and chemical bonding, of the Sn doped PbX (X=S, Se, Te) are calculated by full potential linearized augmented

plane wave method (FP-LAPW) within density functional theory (DFT). The Sn doping concentration for Pb_{1-x}Sn_xS, Pb_{1-x}Sn_xSe, and Pb_{1-x}Sn_xTe is in the range x=0 to x=1 in step of 0.25 in the rock salt phase. By doping Sn in PbX(X=S, Se, Te) the lattice constants decreases linearly by increasing the concentration. The electronic properties also changes with respect to the composition of the materials. The band gap plots of PbX (X= S, Se, Te) show the direct band gap (L-L) nature. The direct band gap is found to vary by doping Sn in PbX(X=S, Se, Te). So the direct band gap of the ternary alloys varies in the range 0- 0.8 eV. It has observed that the s, p and d states of PbX (X=S, Se, Te) control their

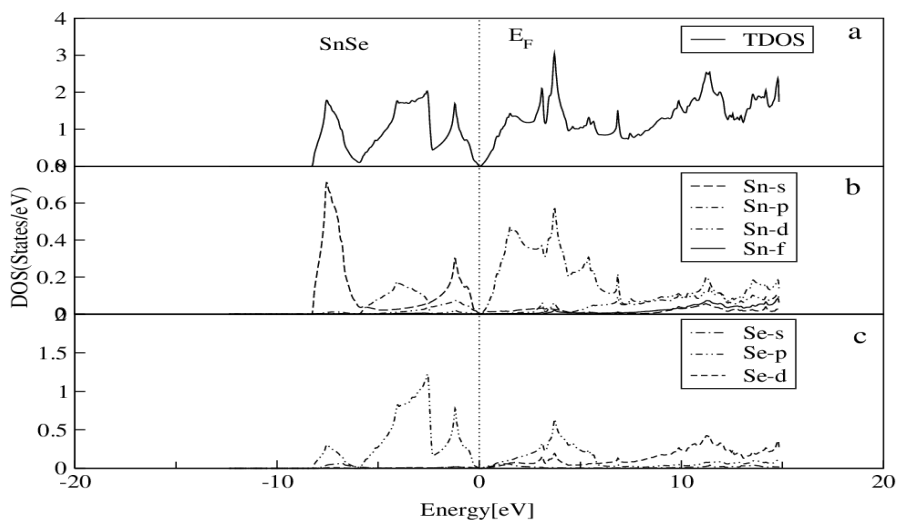


Figure 9: DOS of SnSe.

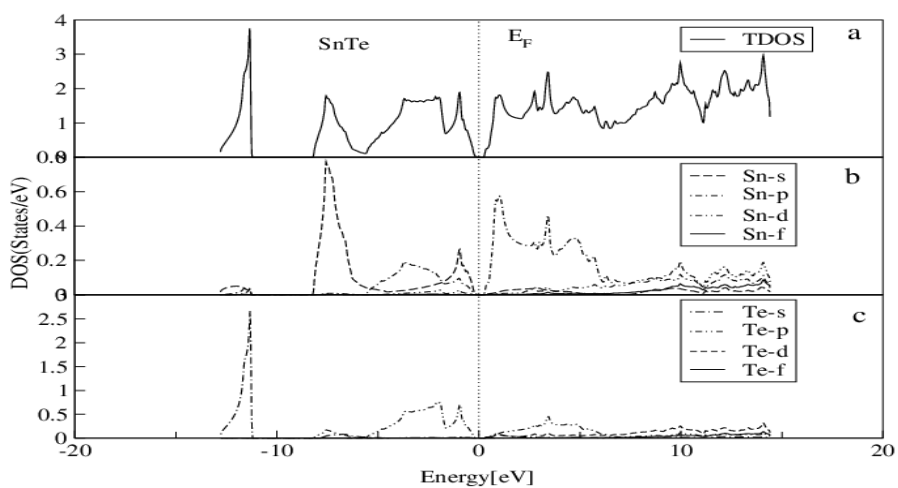


Figure 10: DOS of SnTe.

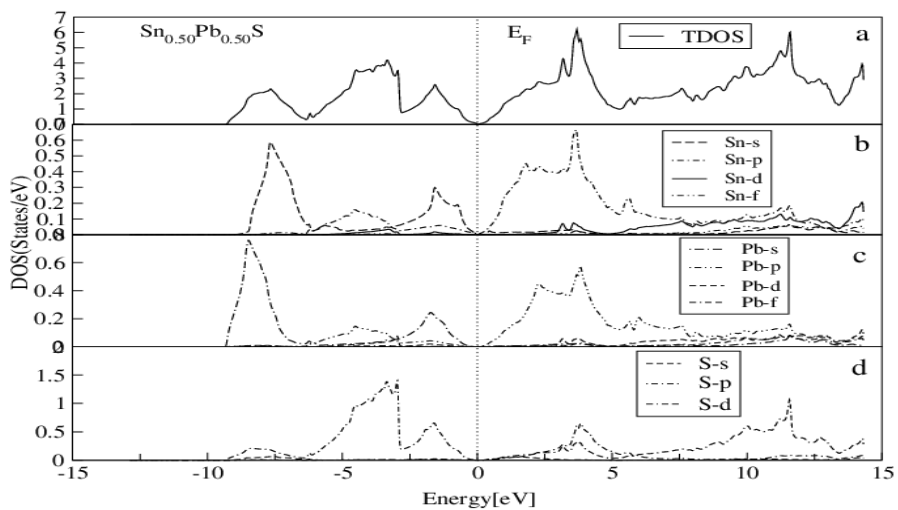


Figure 11: DOS of $\text{Sn}_{0.50}\text{Pb}_{0.50}\text{S}$.

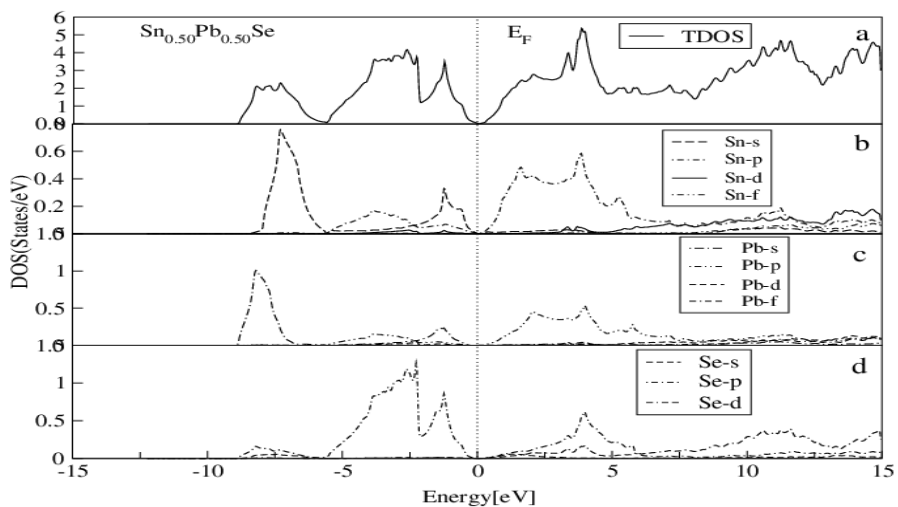


Figure 12: DOS of $\text{Sn}_{0.50}\text{Pb}_{0.50}\text{Se}$.

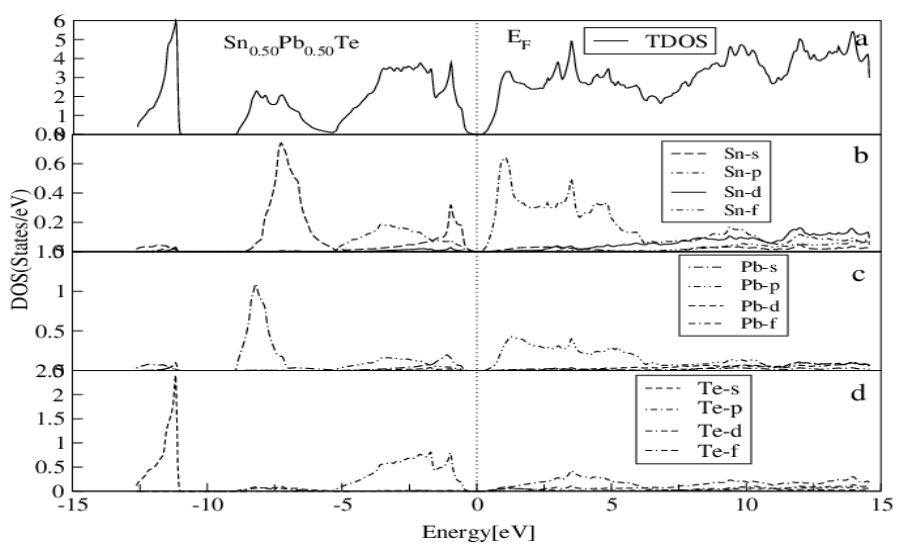


Figure 13: DOS of $\text{Sn}_{0.50}\text{Pb}_{0.50}\text{Te}$.

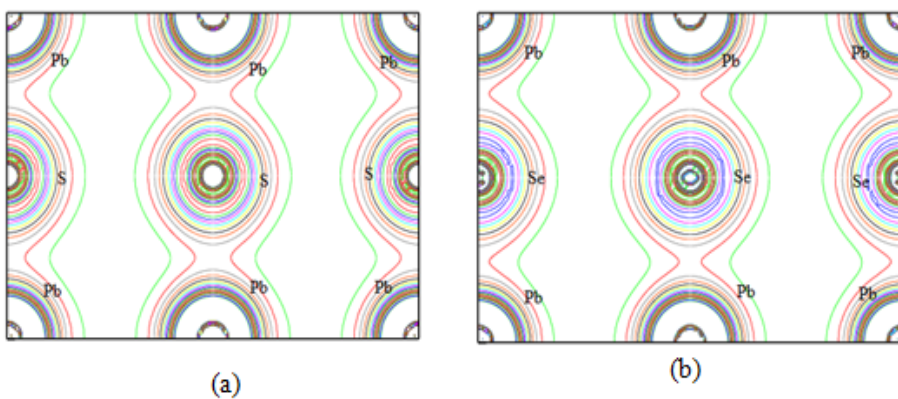
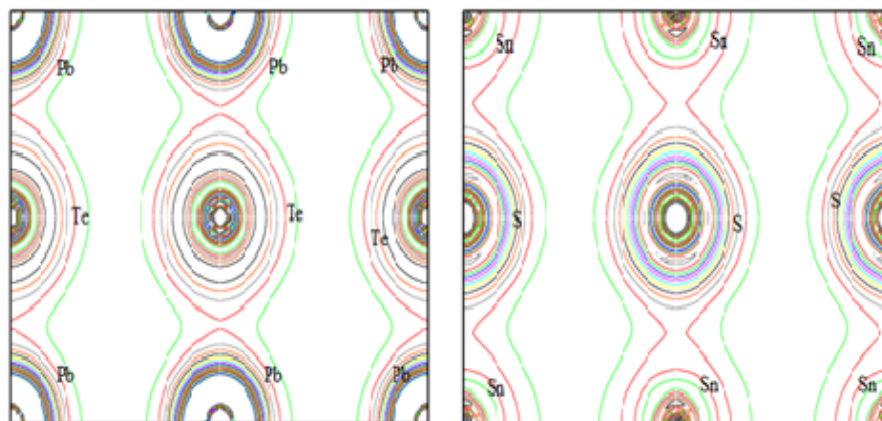


Figure 14(a): Electron charge density of PbS at (110) plane.

Figure 14(b): Electron charge density of PbSe at (110) plane.

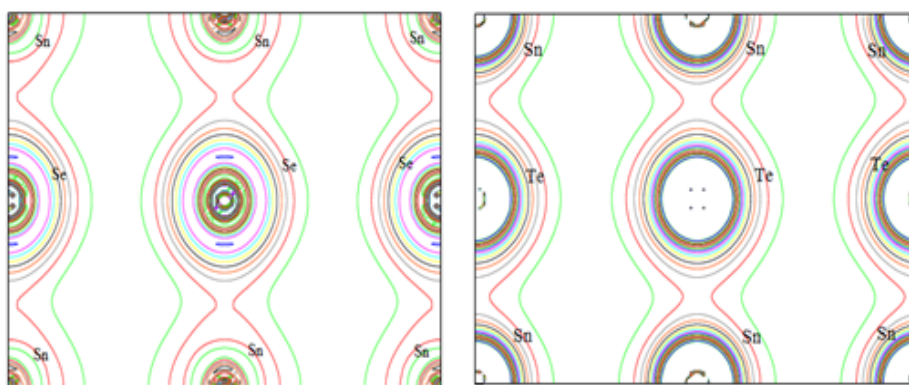


(c)

(d)

Figure 14(c): Electron charge density of PbTe at (110) plane.

Figure 14(d): Electron charge density of SnS at (110) plane.

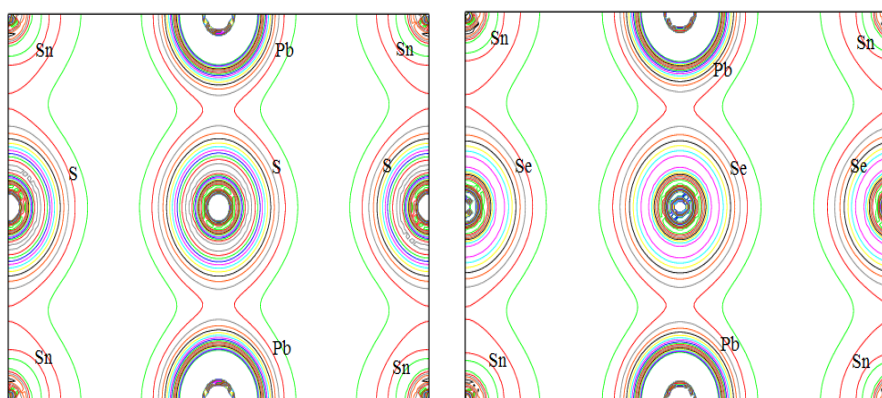


(e)

(f)

Figure 14(e): Electron charge density of SnSe at (110) plane.

Figure 14(f): Electron charge density of PbTe at (110) plane.

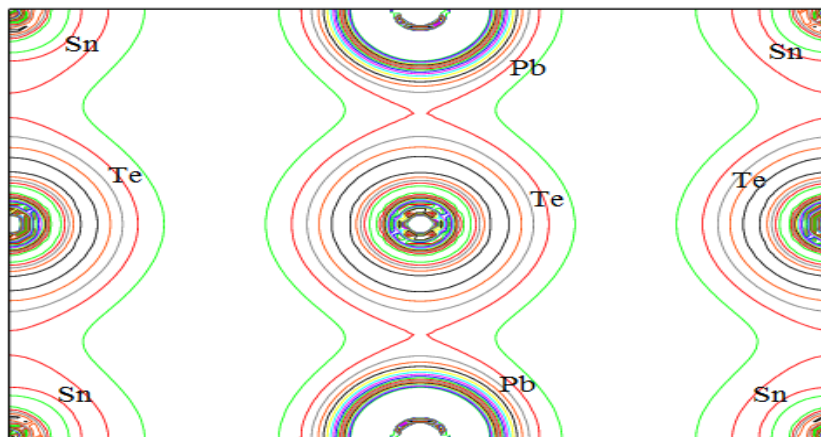


(g)

(h)

Figure 14(g): Electron charge density of Pb_{0.75}Sn_{0.25}S.

Figure 14(h): Electron charge density at (110) plane of Pb_{0.75}Sn_{0.25}Se at (110) plane.



(i)

Figure 14(i): Electron charge density of $Pb_{0.75}Sn_{0.25}Te$ at (110) plane.

electronic properties. The alloys $Pb_{1-x}Sn_xS$, $Pb_{1-x}Sn_xSe$ and $Pb_{1-x}Sn_xTe$ show covalent bonding nature which enhances by increasing the Sn concentration. Hence it is concluded from this study that the Sn doing PbX (X=S, Se, Te) varies the physical properties widely and the resulted materials become more suitable to use in Infrared detectors, Bragg's reflectors and optical devices working in lower frequency regime.

References

- Mun Wong K, Alay-e-Abbas SM, Shaukat A, Fang Y, Lei Y (2013) First-principles investigation of the size-dependent structural stability and electronic properties of O-vacancies at the ZnO polar and non-polar surfaces. *Journal of Applied Physics* 113: 014304.
- Mun Wong K, Alay-e-Abbas SM, Fang Y, Shaukat A, Lei Y (2013) Spatial distribution of neutral oxygen vacancies on ZnO nanowire surfaces: An investigation combining confocal microscopy and first principles calculations. *Journal of Applied Physics* 114: 034901.
- Braun F (1874) On Current Flow through Metallic Sulfides. *Annalen der Physik und Chemie* 153: 556.
- McCann PJ (2006) IV–VI semiconductors for mid-infrared optoelectronic devices. *In Mid-infrared Semiconductor Optoelectronics* 237-264.
- Preier H (1979) Recent advances in lead-chalcogenide diode lasers. *Applied Physics A: Materials Science & Processing* 20: 189-206.
- Zogg H, Fach A, Maissen C, Masek J, Blunier S (1994) Photovoltaic lead-chalcogenide on silicon infrared sensor arrays. *Optical Engineering-Bellingham* 33: 1440-1449.
- Chaudhuri TK (1992) A solar thermophotovoltaic converter using PbS photovoltaic cells. *International Journal of Energy Research* 16: 481-487.
- Abe S, Masumoto K, Mochizuki K, Suto K (1994) Growth and characterization of $Pb_{1-x}Ca_xS_{1-y}Se_y$ thin films prepared by hot wall epitaxy. *Journal of Crystal Growth* 144: 54-58.
- Kumar S, Khan MM, Zulfequar M, Husain M (2007) Optical, structural and electrical investigations on $PbTe_{1-x}S_x$ alloys. *Journal of Materials Science* 42: 363-367.
- Qadri SB, Singh A, Yousuf M (2003) Structural stability of PbS films as a function of temperature. *Thin Solid Films* 431: 506-510.
- Paul A, Klimeck G (2011) Atomistic study of electronic structure of PbSe nanowires. *Applied Physics Letters* 98: 212105.
- Leitsmann R, Bechstedt F, Groiss H, Schäßler F, Heiss W, et al. (2007) Structural and electronic properties of PbTe (rocksalt)/CdTe (zinc-blende) interfaces. *Applied Surface Science* 254: 397-400.
- Rajagopalan M, Kalpana G, Priyamvada V (2006) Pressure induced structural phase transition in SnS-An ab initio study. *Bull Mater Sci* 29: 25-28.
- Wiedemeier H, Schnering HG (1978) Refinement of the structure of GeS, GeSe, SnS and SnSe, *Zeitschrift für Kristallographie* 148: 295-303.
- Jain G (2010) Structural and electrical characterization of sintered SnTe films. *Chalcogenide Letters* 7: 197-202.
- Schwarz K, Blaha P (2003) Solid state calculations using WIEN2k. *Computational Materials Science* 28: 259-273.
- Hohenberg P, Kohn W (1964) Inhomogeneous electron gas. *Physical Review* 136: B864.
- Blaha P, Schwartz K, Madsen GK, Kvasnicka D, Luitz J (2001) WIEN2k, A Full-potential linearized augmented plane wave package for calculating crystal properties (User's Guide). Viena, Austria: Tech. Universität Wien 2001.
- Birch F (1947) Finite elastic strain of cubic crystals. *Physical Review* 71: 809.
- Kumar S, Khan MM, Zulfequar M, Husain M (2007) Optical, structural and electrical investigations on $PbTe_{1-x}S_x$ alloys. *J Mater Sci* 42: 363-367.
- Paul A, Klimeck G (2011) Atomistic study of electronic structure of PbSe nanowires. *Applied Physics Letters* 98: 212105.
- Walsh A, Watson GW (2005) Influence of the Anion on Lone Pair Formation in Sn (II) Monochalcogenides: A DFT Study. *J Phys Chem B* 109: 18868-18875.
- Kacimi S, Zaoui A, Abbar B, Bouhafs B (2008) Ab initio study of cubic PbS_xSe_{1-x} alloys. *Journal of Alloys and Compounds* 462: 135-141.
- Bencherif Y, Boukra A, Zaoui A, Ferhat M (2011) High-pressure phases of lead chalcogenides. *Materials Chemistry and Physics* 126: 707-710.
- Waghmare UV, Spaldin NA, Kandpal HC, Seshadri R (2003) First-principles indicators of metallicity and cation off-centricity in the IV-VI rock salt chalcogenides of divalent Ge, Sn, and Pb. *Phys. Rev. B* 67: 125111.
- Thomas LH (1927) The calculation of atomic fields. In: *Mathematical Proceedings of the Cambridge Philosophical Society Proc* 23: 542.
- Nimtz G, Schlicht B (1983) Narrow-gap lead salts. *In Narrow-Gap Semiconductors*. Springer, Berlin.
- Jain G (2010) Structural and electrical characterization of sintered SnTe films. *Chalcogenide Letters* 7: 197-202.
- Zhao F, Ma J, Weng B, Li D, Bi G, et al. (2010) MBE growth of PbSe thin film with a $9 \times 10^5 \text{ cm}^{-2}$ etch-pits density on patterned (111)-oriented Si substrate. *Journal of Crystal Growth* 312: 2695-2698.
- Kumar S, Khan MM, Zulfequar M, Husain M (2007) Optical, structural and electrical investigations on $PbTe_{1-x}S_x$ alloys. *J Mater Sci* 42: 363-367.
- Rached D, Rabah M, Benkhetou N, Driz M, Soudini B (2003) Calculated band structures and optical properties of lead chalcogenide PbX (X=S, Se, Te) under hydrostatic pressure. *Physica B* 337: 394-403.
- Souza Dantas N (2007) Electronic Structure and Optical Properties of PbY and

SnY (Y=S, Se, and Te). Royal Institute of Technology.

Chalcogenides on Si for Mid-IR Detectors and Emitters Including Cavities. Journal of Electronic Materials 37: 213-219.

33. Zogg H, Arnold M, Felder F, Rahim M, Ebner C, et al. (2008) Epitaxial Lead